

**CHAPTER 1:**  
**INTRODUCTION**

**1.1. MOTIVATION**

The inherently parallel nature of optical information processing, coupled with its typically higher bandwidth, confers a potential advantage over conventional electronically-based processing, such as digital signal processing. Photorefractive media store real-time holograms which have memory and can provide high optical gain ( $20 \text{ cm}^{-1}$ ) at moderately low intensities on the order of  $\text{W}/\text{cm}^2$ , characteristics which are useful in the implementation of optical information processing architectures. Photorefractive-based systems can be subdivided in three main categories: optical computing, image processing and signal processing. Examples of optical computing systems include associative memories and correlators [Gabor, '69; Khoury, '94; Neifeld, '93; Staebler, '75; Yu, '94], neural networks [Denz, '99; Gu, '93; Psaltis, '88], and reconfigurable array interconnects [Anderson, '87; Marrakchi, '90; Weiss, '89]. Image processing systems include functions such as image amplification [Hong, '90], image thresholding [Klein, '86a; Sayano, '88], edge enhancement [Feinberg, '80; Joseph, '92], amplifying spatial filtering [Chang, '90; Fainman, '86], novelty filters [Anderson, '89; Khoury, '91; Uesu, '95]. Narrow-band filters [Hong, '93; Rakuljic, '93] and optical heterodyning [Hamel de Monchenault, '88; Khoury, '93] are examples of signal processing systems. Photorefractive systems applications have been reviewed in [Gunter, '88].

The emphasis in our research group is to perform information processing by use of photorefractive oscillating architectures which we call “rings”, such as the flip-flop [Anderson, '91], the bistable ring [Lininger, '90], the demultiplexer [Saffman, '91], and the feature extractor [Anderson, '92]. These demonstrations are described as “self-organized”, for the reasons that no external programming of the photorefractive ring is needed, nor is any *a priori* information about the input signals, except for the requirement that they be both temporally and spatially orthogonal. The dynamics of a ring oscillator generate real-time volume holograms in the photorefractive crystals which we call gratings. The competition dynamics between the generated gratings allow for different algorithms, such as separating temporally uncorrelated signals in different rings in the demultiplexer, or extracting the principal component within the input signals in the feature extractor.

This thesis focuses upon a fundamental functional unit in photorefractive processing: the two-beam coupling interaction. It is the main functional unit from which the ring systems are built, and it is also used in many of the more general applications mentioned above, such as in image amplifiers, novelty filters, notch filters, and others.

The next couple chapters in this thesis are motivated by the importance of developing a more component oriented technology for photorefractive functions, as it will significantly contribute to making photorefractive system testing and building more practical. Its widespread use in photorefractive systems justifies the choice of two-beam coupling as the example-function for testing such technology. Naturally, the same concept can be used for other photorefractive functions as well, such as

phase conjugation or four-wave mixing. The role that the development of such a component technology could represent to photorefractive systems can be illustrated by drawing an analogy with electronic systems, where systems can be assembled by the use of chips with a wide variety of function, canceling the need of building the system from the transistor level. For this purpose, in chapter 2, we introduce a modular design, where each module is pre-aligned to perform a particular photorefractive function, and the modules are interconnected by multimode optical fibers. Such technology allows systems containing several modules to be easily assembled and re-configured without the need of any system alignment. Each module is built for a specific desired function – a two-beam coupling module built for gain will be optimized differently than one built for novelty filtering. In the end of chapter 2, we give an application example using such modules. There we show how their use allowed a quick and easy verification of the change in behavior of a ring system when an extra module is inserted into its feedback loop, sparing the need for tedious realignment on the conventional optical table.

In chapter 3, we introduce the use of spherical photorefractive crystals. Their original purpose was in developing more compact two-beam coupling units. Due to the curvature and high refractive index of the crystal, no other optical elements are necessary for these modules except for the input and output fibers and the crystal itself. A built example of such module is shown herein. Interestingly, when testing the spherical crystals, we found that a single pump beam generated oscillating patterns within the crystal. These patterns arise from total internal reflections within the crystal, forming closed-path oscillating modes, known as whispering-gallery

modes. A spherical disk, an equatorial slice of the sphere containing the crystal's uniaxial, the "c-axis", was produced to allow better visualization of the patterns. The occurrence of the strongest mode, the triangle pattern, was mapped as a function of pump input and c-axis angles. A simple theory, assuming pumping of the modes by means of a single two-beam coupling interaction, resulted in good qualitative agreement with the experimentally obtained mapping. Due to the lack of a phase conjugate of the pump-beam, we believe that the oscillations are unidirectional, meaning that these structures are miniature analogues of unidirectional ring oscillators pumped by a two-beam coupling interaction, which is the architecture used for several of our signal processing systems, such as the feature extractor.

As mentioned above, the ring processors developed in our laboratories typically require that the input signals be temporally and spatially orthogonal. However, when using electrooptic modulators to impose a temporal signal upon different optical beams, the signals in these beams will have a correlation term due to the common carrier. Therefore, for the ring processor to function properly, it becomes necessary to remove the optical carrier from each signal beam. This is the case for a system being currently developed, the "optically-smart antenna array", which we describe in more detail in chapter 4. This system contains a feature extractor, currently renamed as the "autotuning filter", whose purpose is to select the strongest signal within the several signals presented at its input. Because the optical signals in this system are generated by using an electrooptic modulator, for the reason just explained above, a carrier suppressor is needed in front of the filter's input. Once again, two-beam coupling proves its versatility by performing adaptive carrier

suppression when used in a novelty-filter configuration. Carrier suppression of more than 70 dB is demonstrated. Such results were possible due to the development of an operator formalism which is the subject of the last chapter. In chapter 4, we provide a simplified, geometrical picture of this operator theory applied to the carrier suppression problem. This geometrical picture provided a greater intuitive understanding of the suppression mechanism, and allowed us to set the parameters involved in the carrier suppressor, such as input intensity ratio of the beams and the modulation strength.

Finally, the last chapter describes the operator algebra formulation for two-beam coupling. In 1979, Kukhtarev published a theoretical model for beam coupling which employed coupled wave theory [Kogelnik, '69] taking into account the effect of self-diffraction of light induced gratings. [Kukhtarev, '79] The equations presented in the next section are based on the plane-wave approximation to this theory, considered the foundation for two-beam coupling modeling. However, as the number of plane-waves interfering in the crystal increases, this theory becomes increasingly more difficult and awkward to deal with. A generalized operator algebraic theory, for which the input beams can be cast not only on a plane-wave basis, but on any set of orthogonal spatial bases is then indicated. The operator theory presented in chapter 5 treats the photorefractive medium as a black box described by a coupling operator  $T$ , which acts upon an input field vector to produce the output field vector,  $\mathbf{E}(out)=T\mathbf{E}(in)$ . The field vectors are represented in whichever basis is better suited to the information processing task at hand. Due to this freedom in representing the information, the operator theory bridges a gap between the physics of two-beam

coupling and its theoretical-computational representation, leading to a deeper intuitive understanding of the beam coupling phenomena. In fact, this is exemplified in chapter 4, section 4.4, where a geometrical picture of the operator formalism led to the prediction of carrier suppression features by simply graphically representing the field vectors and studying the action of  $T$  upon these vectors. In the last chapter, we present the analytical solution for the coupling matrix  $T$  for the case of one spatial mode in each of the two input beams. We present the “complex-coupling” solution, which corresponds to the general case consisting of a combination of intensity coupling (real case) and phase coupling (imaginary case).

Before proceeding to chapter 2, in the next section we present a brief summary of two-beam coupling, for those readers who are not familiar with the process.

## **1.2. TWO-BEAM COUPLING: AN OVERVIEW**

This overview is just that, an overview, where an effort is made to only cover the main aspects of two-beam coupling necessary for the understanding of the following chapters. We explain the physical phenomenon behind the two-beam coupling process and introduce the two-beam coupling equations. For more detailed accounts we refer the reader to [Solymar, '96; Yeh, '93].

Two-beam coupling is a nonlinear optical interaction that can transfer energy or phase information between two overlapping beams in a photorefractive medium.

The two-beam coupling medium of this thesis is always an electrically unbiased, open-circuit, barium titanate ( $\text{BaTiO}_3$ ) crystal, where the charge transport is primarily due to diffusion, resulting in a pure energy transfer process [Buse, '97]. Barium titanate displays high two-beam coupling gain over a wide wavelength range. (Barium titanate is a perovskite ferroelectric material belonging to the 4mm crystallographic group symmetry. It's photorefractive properties are widely available in the literature. [Klein, '86b; Mazur, '99].)

A two-beam coupling diagram is shown in figure 1.1. Two beams cross inside a crystal forming an interference pattern, which is sinusoidal if the beams are assumed to be plane waves. The bright regions of the interference pattern can excite charge carriers from impurity donors, typically iron ions ( $\text{Fe}^{2+}$  and  $\text{Fe}^{3+}$ ) in barium titanate, to the conduction band. In this model we assume the only charge carriers are electrons. The electrons in the conduction band are free to migrate whereas the ionized donors are fixed to the crystal lattice. Electrons may experience several transitions as they migrate, in other words, they are re-combined with the ionized donors and re-excited to the conduction band. Because the excitation of the electron is proportional to the light intensity, more electrons are generated in the bright regions as opposed to the dark regions of the interference pattern. This causes an average migration or diffusion of electrons to the dark regions. This charge separation results in a charge density function ( $\rho$ ) with the same periodicity of the interference pattern, as shown in figure 1.2. The charge density and the resulting space-charge field ( $E_{SC}$ ) are related by Poisson's equation,  $\epsilon E_{SC} = \rho$ , which introduces a  $90^\circ$  phase shift between  $\rho$  and  $E_{SC}$ .

Barium titanate displays a strong linear electrooptic effect, also known as Pockel's effect, which generates a refraction index grating in the medium which mimics the space-charge field. The optical fields which originally recorded this grating will now scatter from it, i.e., the fields experience self-diffraction. The  $90^\circ$  phase shift between the index grating and the interference pattern causes the diffracted beams to interfere constructively in one output direction (along the "gain beam") and destructively in the other output direction (along the "loss beam"). This results in an energy transfer between the beams. The direction of energy transfer is determined by the crystal's optical axis. We designate the beam that loses energy as the "loss beam", and the one that gains energy, the "gain beam". For a given purpose, sometimes the gain beam is the pump, sometimes it is the signal. Typically it is easier to follow the pump and signal paths, though the gain and loss never change.

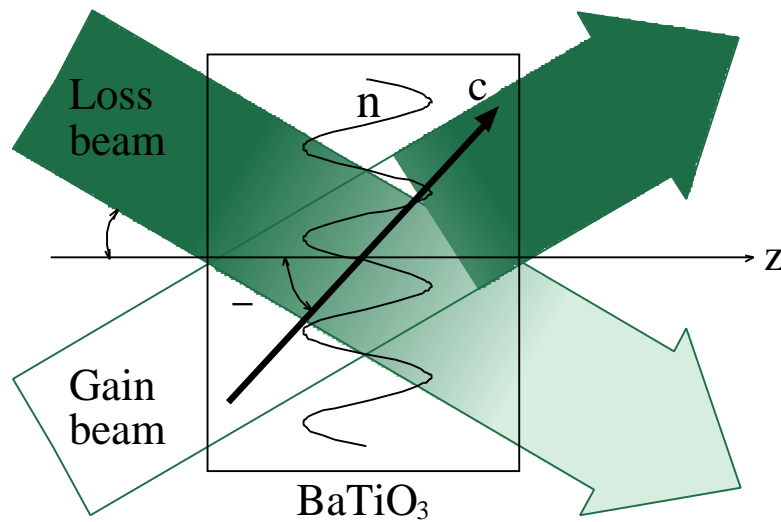


**Figure 1.1.** Two-beam coupling diagram. Loss beam transfers energy to gain beam. The direction of energy transfer is determined by the c-axis direction and the sign of the charge carriers. Higher gray level saturation implies brightness of the beams.

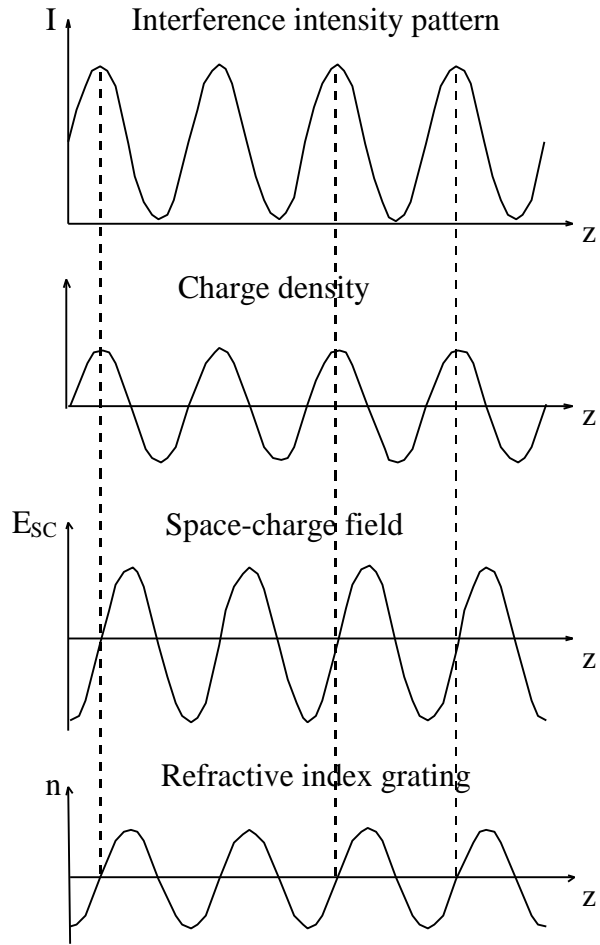


**Figure 1.2.** The photorefractive effect. The intensity pattern from two interfering beams create a charge separation with the same periodicity and shape as the intensity variation. The associated space-charge field, which is shifted by  $90^\circ$  when no external fields are applied, induces an index grating in the medium via the linear electrooptic effect (Pockel's effect).

In steady-state, the energy transfer process is represented by the following two-beam coupling differential equations with respect to the propagation direction  $z$ :

$$\begin{aligned}\frac{dA_1}{dz} &= G A_2 \\ \frac{dA_2}{dz} &= -G A_1\end{aligned}\quad [1.1]$$

where  $G$  represents the grating strength:

$$G = \frac{1}{2I_0} \gamma A_1 A_2^*, \quad [1.2]$$

and  $I_0 = |A_1|^2 + |A_2|^2$  is the total intensity. The gain coefficient  $\gamma$  depends upon the material properties of the crystal and upon the geometrical arrangement of the setup, and is given by:

$$\gamma = \frac{2\pi}{n\lambda \cos\theta} r_{eff}, \quad \text{where } r_{eff} = -2n_o^2 n_e^2 r_{42} E_{sc}(\theta, \alpha) \cos\alpha \sin(2\alpha). \quad [1.3]$$

In the expression above,  $r_{eff}$  is the effective electrooptic coefficient,  $\lambda$  is the wavelength in air of the input beams,  $\theta$  is the half-angle between the two beams,  $\alpha$  is the angle between the beams's bisector and the c-axis, and  $n_o$  and  $n_e$ , the ordinary and extraordinary index of refraction ( $n_o = 2.437$ ,  $n_e = 2.365$ ). The  $r_{eff}$  depends on the polarization state of the fields. In this treatment we only take into account the main component of barium titanate's electrooptic tensor ( $r_{42}=1640$  at low frequencies), since the other components are more than one order of magnitude smaller. For

extraordinary fields, this term is proportional to  $\cos\alpha\sin2\alpha$ . Additionally, the space-charge field is a function of both  $\theta$  and  $\alpha$ .

$$E_{SC} = \frac{iK \frac{k_B T}{q}}{1 + \frac{K^2}{k_D^2}} \quad [1.4]$$

It depends on  $\theta$  through the wave vector  $K = \frac{4\pi n}{\lambda} \sin\theta$ , and on  $\alpha$  through the Debye screening length  $k_D$ , which in turn depends on the effective dielectric constant  $\langle \epsilon \rangle = \epsilon_{//} \cos^2 \alpha + \epsilon_{\perp} \sin^2 \alpha$ , where  $\epsilon_{//}$  and  $\epsilon_{\perp}$  are the DC dielectric constant for an electric field parallel and perpendicular to the c-axis, respectively. Barium titanate displays a high dielectric anisotropy with  $\epsilon_{//} = 135$  and  $\epsilon_{\perp} = 3600$ .

Solving the above equations, we get the following expressions for the intensities of the gain-beam  $I_1$  and the loss-beam  $I_2$ :

$$\begin{aligned} I_1(z) &= I_1(0) \frac{1+m}{1+me^{-\gamma z}} \\ I_2(z) &= I_2(0) \frac{1+m^{-1}}{1+m^{-1}e^{\gamma z}} \end{aligned} \quad [1.5]$$

where  $m$  is the input intensity ratio  $I_2(0)/I_1(0)$ .

Using the above equations, we plot in figure 1.3 the gain and loss beam intensities as they propagate through the crystal, for different values of the gain coefficient, 5, 10 and 20  $\text{cm}^{-1}$ , and a input intensity ratio of 100. As expected, energy transfer occurs earlier for higher gain coefficients.

## Energy transfer in two-beam coupling

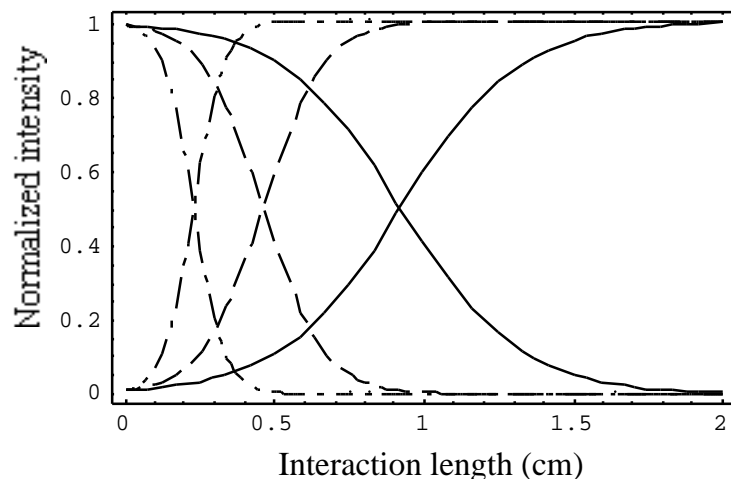


**Figure 1.3.** Normalized intensity plots of gain and loss beam pairs,  $I_1(z)$  and  $I_s(z)$  for  $=5 \text{ cm}^{-1}$  (solid curve),  $10 \text{ cm}^{-1}$  (dashed curve), and  $20 \text{ cm}^{-1}$  (dash-dot curve). The input intensity ratio is set at 100.

Besides the gain, two other parameters are important for evaluating coupling process. The first one is losses, which can be divided into passive losses and active losses. Passive losses are due to surface reflections and absorption in the crystal. Absorption is not taken into account in the above expressions. To account for it, one simply multiplies equations [1.5] by  $e^{-\alpha z}$ , where  $\alpha$  is the absorption coefficient. The curves in figure 1.3 would then be weighed by an exponential decay as they propagate in  $z$ . The active losses are due to scattered light from impurities and defects from the crystal, which are amplified by the photorefractive gain, forming what is called “fanning”. A picture of fanning simulation is shown in figure 1.4, after the work from [Zozulya, '95]. The losses due to fanning may be reduced by aligning the crystal in the direction of the beam fan, but the trade-off is reduced output signal dynamic range.

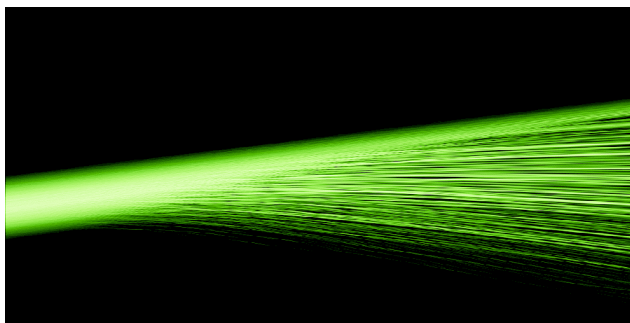


**Figure 1.4.** Spatial structure of fanning light inside a crystal.

The gratings in a photorefractive crystal adapts to the average input signals integrated over the time constant (  $\tau$  ) of the crystal. The inverse time constant of barium titanate is typically between 1-100 Hz. One might question whether such a slow response doesn't significantly limit the applicability of the photorefractive processors. In some applications, such as phase-conjugation, reconfigurable interconnections and in some image processing systems, a fast photorefractive response is desirable. However, for our applications the slow response time is not a limiting factor, but in fact actually advantageous as it allows signals which are merely  $1/\tau$  apart in frequency to be distinguished by the system. In some of these applications, the slow time constant results in long term statistical correlations which allow the system to distinguish even between signals with overlapping bandwidths. For instance, the signals could consist of speech. The speech from a particular person may vary on a short-time scale, however, on a longer time scale a person's speech is more correlated with itself than with another's, which is the key property that allows the speakers to be separated [Min, '88]. On the other end, the upper frequency limit

for the signals in the photorefractive processors is given by Bragg matching considerations and is a few gigahertz for a 1 cm grating. This limit is inversely proportional to the grating length.